

#### Contents lists available at ScienceDirect

# Fuel

journal homepage: www.elsevier.com/locate/fuel



### Full Length Article

# Charge characteristics of sub-10 nm soot particles in premixed ethylene flames



Mengda Wang<sup>a,b</sup>, Girish Sharma<sup>c</sup>, Huang Zhang<sup>c</sup>, Xiaoqing You<sup>a,b,\*</sup>, Pratim Biswas<sup>c,\*</sup>

- <sup>a</sup> Center for Combustion Energy, Tsinghua University, Beijing 100084, China
- b Key Laboratory for Thermal Science and Power Engineering of the Ministry of Education, Tsinghua University, Beijing 100084, China
- <sup>c</sup> Aerosol and Air Quality Research Laboratory, Department of Energy, Environmental & Chemical Engineering, Washington University in St. Louis, St. Louis, MO 63130, IISA

#### ARTICLE INFO

# Keywords: Nascent soot Charged PSDs Charge fraction Premixed ethylene flames

#### ABSTRACT

In this work, the charge characteristics of sub-10 nm soot particles were studied in burner-stabilized-stagnation premixed ethylene flames, at an equivalent ratio of 2.0 and over the calculated maximum flame temperature ( $T_{\rm max}$ ) range of 1665–1933 K, using micro-orifice probe sampling in tandem with neutralizer, half-mini differential mobility analyzer (Half-mini DMA) and electrometer. To obtain the charge fraction, the charged and total particle size distributions (PSDs) were measured with the neutralizer off and on, separately. Our results showed that both negatively charged particles (NCP) and positively charged particles (PCP) grew to bigger particles with the increase of height above burner ( $H_{\rm p}$ ). However, compared to PCP, NCP were relatively smaller in size, but higher in concentration, possibly because negative ions such as electrons diffused faster to coagulate with soot. Moreover, charge fraction decreased along  $H_{\rm p}$  and newly nucleated soot particles were all neutral at higher  $H_{\rm p}$ , which could be attributed to the higher temperature near the flame front, where the concentrations of ions were higher. Another interesting finding was the increase in charge fraction by two orders of magnitude (from 0.1% to 10%) as  $T_{\rm max}$  increased from 1665 K to 1933 K. All of these suggested the existence of particle-ions interaction close to the flame front, especially at high temperatures.

## 1. Introduction

Ions formed in high temperature flames may affect soot formation processes [1-6]. On one hand, they can enhance particle coagulation by colliding with soot particles [7–10]. On the other hand, they may serve as the initial soot precursor for generating incipient soot [11]. Since ions may play an important role in soot formation, they have received substantial attention for decades. Calcote et al. [11] suggested that precursor ions such as C<sub>3</sub>H<sub>3</sub> + could react with neutral species, for example acetylene, to produce larger positive ions and charged particles. Lias et al. [12] showed that ion-molecule reaction rate coefficients were generally several orders of magnitude greater than those of neutral species, and ion-molecule reaction rates were fast in high-temperature sooting flames. Kraft and coworkers [13,14] proposed that enhanced interactions between polar corannulene molecules and cations resulted in more rapid and abundant clustering and longer cluster life times, suggesting that interactions between curved PAHs and ions may play a significant role in soot formation. In contrast, Haynes et al. [15] argued

that concentrations of ions were too low to play a major role in soot formation.

To investigate the effect of ions on nucleation and coagulation, it is necessary to study the charge characteristics of soot particles. Maricq [16] measured the charged particle size distributions (PSDs) and charge fractions of soot particles in premixed ethylene flames by nano-differential mobility analyzer (DMA) and condensation particle counter (CPC). The results showed that nanoparticles carried predominantly with a single charge and the charge fraction increased with the increase of size. Due to the low activation efficiency of CPC and high diffusion loss of nano-DMA for sub-3 nm particles [17,18], measurements were performed only for particles larger than 3 nm. To shed light on sub-3 nm soot particles, Sgro et al. [19,20] used a higher resolution TapCon DMA coupled with an electrometer to investigate charged particles. However, these works focused on the positively charged particles and no results of negatively charged particles were reported. Besides, the diffusion loss was still too high and the resolution was still too low to get accurate data for sub-3 nm particles. These limitations have

E-mail addresses: xiaoqing.you@tsinghua.edu.cn (X. You), pbiswas@wustl.edu (P. Biswas).

<sup>\*</sup> Corresponding authors at: Center for Combustion Energy, Tsinghua University, Beijing 100084, China (X. You). Department of Energy, Environmental & Chemical Engineering, Washington University in St. Louis, MO 63130, USA (P. Biswas).

Nomenclature		$Q$ Flow rate of samples in the electrometer $T_{\rm max}$ Calculated maximum flame temperature	
CPC	Condensation particle counter	T-NCP	Total PSDs inferred from measurement of negatively
DMA	Differential mobility analyzer		charged particles
e	Electronic charge	T-PCP	Total PSDs inferred from measurement of positively
$H_{\rm p}$	Height above burner		charged particles
$I_{ m EM}$	Electrometer current	$\eta_{ m neu}$	Neutralizer charging efficiency
N	Total particle number concentration	$\eta_{ m Diff}$	Penetration efficiency of the neutralizer and connection
NCP	Negatively charged particles		tubes
PCP	Positively charged particles	$\eta_{ m DMA}$	Penetration efficiency of the Half-mini DMA
PSD	Particle size distribution		

hindered the discovery of charge characteristics for sub-3 nm particles.

To counteract the diffusion broadening of DMA transfer functions, de la Mora [21,22] designed high resolution DMA (Half-mini DMA) with new configurations and with sheath flow rates over 100 lpm, which significantly reduced the residence time and diffusional loss of classified particles. By applying an electrometer downstream of the Half-mini DMA, Wang et al. [23–25] measured the concentrations of classified sub-3 nm particles successfully. Thus, the combination of Half-mini DMA coupled with an electrometer may serve as a powerful tool in studying the charge characteristics of soot particles below 3 nm.

In this work we investigated the charge characteristics of nascent soot (sub-10 nm) particles in burner-stabilized-stagnation premixed ethylene flames, using micro-orifice probe sampling in tandem with neutralizer, Half-mini DMA and electrometer. With the neutralizer on, total PSDs (including both charged and neutral particles) were obtained by measuring both positively charged particles (PCP) and negatively charged particles (NCP) coming out of the neutralizer. With the neutralizer off, the PSDs of natural positively and negatively charged particles from flames were measured. Considering that ions may be significantly affected by flame temperature, we studied the size-dependent charge characteristics of sub-10 nm soot particles at different flame temperatures.

#### 2. Experimental

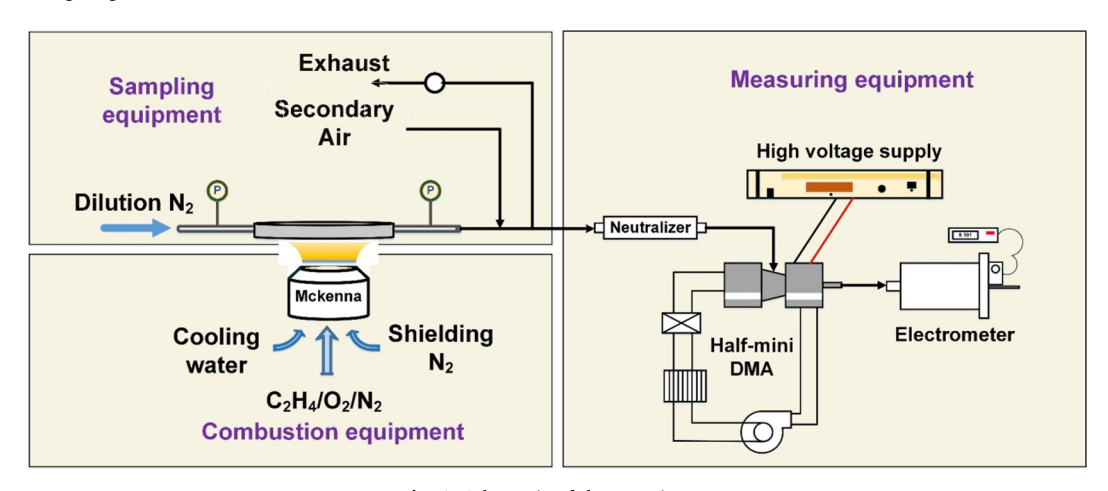
The experimental setup is shown in Fig. 1. It consists of burner-stabilized-stagnation flames, a high-dilution sampling system and sub-10 nm particle measurement instruments. The burner-stabilized-stagnation flames and the sampling probe are the same as those in our previous studies [26–28] while the combination of a Half-mini DMA and an electrometer is used to measure sub-10 nm particles.

Firstly, flames are generated by a commercial McKenna burner with a stainless outer layer and a 60-mm diameter bronze porous sintered plug. A shroud nitrogen gas, at 25–30 cm/s, shields the flame from

surrounding air. A stainless steel sampling tube with a 0.16 mm sampling orifice is embedded in the stagnation plate. To extract soot samples into the sampling tube through orifice, the downstream of the sampling tube is attached to a vacuum pump to maintain a negative pressure at the sampling orifice. Soot particles are drawn into the sampling tube through the orifice and are diluted immediately by a 30 L/min nitrogen flow in the tube. The detailed sampling set-up is described in Ref [28]. The appropriate dilution ratio (~1100) has been determined and used in this work for eliminating chemical reactions and particle coagulation in the sampling tube. The reliability of this sampling system has been proved by the highly consistent results from three research groups [26]. Besides, the detailed calibration and uncertainty analysis of our sampling equipment has been shown and verified in Ref. [26].

To study the charge characteristics of flame-generated soot particles, it is necessary to measure the PSDs for both charged and total (including both charged and neutral) particles. The total PSDs were measured by a neutralizer-Half-mini DMA-electrometer system, while the charged PSDs were measured using the Half-mini DMA and electrometer without a neutralizer.

When measuring the total PSDs, the laminar flow bipolar diffusion neutralizer was used to charge sample particles to produce a known Fuchs' stationary-state charging distribution [29]. The neutralizer in this study is a commercial radiative charger. The ionization source is Po<sup>210</sup>. Subsequently the Half-mini DMA was used to classify sub-10 nm particles. To balance the sample inlet and outlet flows and to maximize the instrument resolution, the Half-mini DMA was operated in a closed-loop configuration, recirculating high purity nitrogen in the sheath flow. The high negative and positive voltages controlled by LabVIEW were applied on the two electrodes of the DMA to classify positive and negative particles, separately. After being classified by the Half-mini DMA, the charged particles were introduced to an aerosol electrometer operated at a flow rate of 5 lpm. As the multi-charged sub-10 nm particles after the neutralizer were negligible [30], the particle



 $\textbf{Fig. 1.} \ \textbf{Schematic of the experiment.}$ 

concentrations were directly proportional to the current measured by the electrometer. The electrometer current data were collected by the LabVIEW through RS-232 communication. Thus, the total particle number concentration, N, can be obtained by Eq. (1),

$$N = \frac{I_{EM}}{e \cdot Q} \cdot \frac{1}{\eta_{DMA}} \cdot \frac{1}{\eta_{Diff}} \cdot \frac{1}{\eta_{neu}}$$
(1)

where  $I_{\rm EM}$  is the electrometer current, e is the electronic charge, Q is the flow rate of soot samples in the electrometer,  $\eta_{\rm DMA}$  is the penetration efficiency of Half-mini DMA,  $\eta_{\rm Diff}$  is the penetration efficiency of neutralizer and connection tubes,  $\eta_{\rm neu}$  is the neutralizer charging efficiency. The first term on the right side of Eq. (1) indicates the number of singly-charged particles per unit volume in the classified aerosol reaching the electrometer; the second term stands for particle loss in DMA; the third term denotes particle diffusion losses through tubes; and the fourth term signifies Fuchs' stationary-state charging distribution of the neutralizer.

As mentioned above, when measuring only the charged particles in flames, the sample particles were introduced directly into the Half-mini DMA to classify sub-10 nm charged particles, as the neutralizer was no longer necessary.

In this work, the evolution of total and charged PSDs at different heights above the burner  $(H_p)$  were measured, since ion concentrations may vary with heights [3,12]. Moreover, considering that ion concentrations and components might be affected by the flame temperature, we examined three flames with different calculated maximum flame temperatures ( $T_{\rm max}$ ) by changing the cold gas velocity but keeping the unburned gas composition the same, i.e., 16% (mol) ethylene, 24% (mol) oxygen and 60% (mol) nitrogen at an equivalence ratio of 2.0. Table 1 summarizes the conditions of the three flames. The flame temperatures at different burner-to-stagnation separation distances were computed using the Premixed Laminar Burner-Stabilized Stagnation Flame module from Chemkin-Pro [31] and the kinetic model of USC Mech II [32]. The boundary temperature on the burner side was set the same as the temperature of the burner chiller (298 K), and that on the stagnation plate side was measured by a type-K thermocouple, which was about 465 ± 30 K. The windward differencing, thermal diffusion and multicomponent transport were adopted. Because previous investigations on a series of premixed ethylene flames showed that the measured flame temperatures agreed well with the modeling results [26-28], we only measured the temperature profile of Flame A2 at  $H_D = 0.45$  cm to verify the reliability of simulation results by an Stype thermocouple coated with Y/Be/O mixture in this work. The computed and experimental temperature profiles agree well as shown in Fig. S1 of the Supplemental Material.

#### 3. Results and discussion

Fig. 2 shows the PSDs in Flame A2 measured with a neutralizer. Soot particles passing through the neutralizer were assumed to follow the Fuchs' steady-state charge distribution. The total PSDs were inferred from measurements of either positively charged particles or negatively charged particles, and they are termed as T-PCP and T-NCP, respectively. Each point in Fig. 2 is an average of at least three repeated experimental results. Due to the existence of negative ions below 1.6 nm and positive ions below 1.8 nm from the neutralizer as shown in Fig. S2 in the Supplemental Material, the total PSDs data were cut off at these two lower limits. In general, the total PSDs (i.e. T-PCP and T-NCP) followed log-normal distributions. The lowest  $H_p$  for finding soot particles larger than 1.6 nm is at  $H_p = 4.0$  mm, where nucleation was initiated as only a few sub-3 nm soot particles were found. With the increase of  $H_p$ , soot particles grew bigger due to particle coagulation. Moreover, small particles near cut-off sizes were found at all  $H_{\rm p}$ , implying the persistent nucleation along with the growth of particles. It was noteworthy that the T-PCP and T-NCP respectively matched well

when particles were larger than 2.0 nm, however, differed much when particles were smaller than 2 nm. This indicated that the Fuchs' steady-state charge distribution was only suitable for describing particles larger than 2 nm. As a matter of fact, the accuracy of the theory of Fuchs on charging 2–100 nm particles by neutralizer has been verified by charging monodisperse nanoparticles such as sodium chloride and silver particles in atmospheric air, argon and nitrogen [33–35]. Soot particles smaller than 2 nm failed to follow the Fuchs' steady-state charge distribution in the neutralizer, which was very likely due to the low charging efficiency between neutralizer ions and sub-2 nm soot particles. As reported by Ref [35], charging efficiency decreased significantly with the decrease of particle size and reached below 1% for sub-2 nm particles. Hence, a more effective charging method for sub-2 nm particles should be utilized in future work.

The evolution of the charged PSDs of Flame A2 is shown in Fig. 3. In general, both of PCP and NCP grew to bigger particles with the increase of  $H_p$ . The lowest  $H_p$  at which natural charged particles could be found was 3.5 mm and the smallest particles were 1 nm, which was below the lower limit of total PSDs, since there was no disturbance from neutralizer ions in the direct measurement of charged particles in flames. At  $H_p = 3.5$  mm, a flame photo in Fig. S3 in the Supplemental Material showed a soot inception flame appearing light yellow luminosity, which verified the formation of soot particles at this  $H_p$ . With the increase of  $H_{\rm p}$ , the positively charged PSDs kept log-normal distributions with increasing median diameters, while the negatively charged PSDs changed from single modal to bimodal at  $H_p = 4.5$  mm and subsequently changed back to single modal at  $H_D = 5.5$  mm. The multimodal shapes of NCP suggested the occurrence of physical (collisional) clustering of monomers. Such clustering occurred and acted in parallel to the chemical reactions during negatively charged soot growth. By comparison, the positively charged soot mainly grew by chemical reactions which showed a unimodal distribution. Besides, compared to PCP, NCP were relatively smaller in size, but higher in concentration at all  $H_p$ . This phenomenon may be explained by two possible reasons. Firstly, negative ions such as electrons diffused faster to coagulate with soot, leading to smaller and more NCP. Secondly, a faster growth of PCP might cause bigger particles. However, we did not find a higher concentration of newly nucleated NCP compared to PCP at  $H_p = 3.5$  mm. Thus, the first explanation is preferred and we speculate that particle charging by direct impact of electron diffusion [10,36,37] and negative ion diffusion [30] was the dominant mechanism for particles acquiring negative charge, whereas positively charged precursors (PAHs) [3,12] and positive ion diffusion [30] contributed to positive charge on particles.

In addition to the detailed PSDs, Fig. 4 shows the number concentrations of total and charged sub-10 nm soot particles. Each point in Fig. 4 is the mean values of three repeated measurements. The results are highly consistent and the relative error is less than 2%. As shown, the number concentrations of T-NCP and T-PCP were almost the same, except for a slight difference at low  $H_{\rm p}$  due to the neutralizer limit on sub-2 nm particles. Similar to the PSDs results, the number concentrations of total particles increased with  $H_{\rm p}$ , indicating persistent nucleation. By contrast, the number concentrations of charged particles (NCP and PCP) increased only slightly with  $H_{\rm p}$ , which indicated that charged particles were mainly generated at low  $H_{\rm p}$ . The computed temperature profiles at different burner to stagnation distances were shown in Fig. 5. In general, the temperature increased first and then decreased with the increase of  $H_{\rm p}$  and reached the maximum value at 0.1–0.2 cm. At low

Table 1
Summary of flame conditions.

Flame	Cold gas velocity (cm/s)	$T_{\rm max}$ (K)
A1	6	1665
A2	10	1824
A3	15	1933

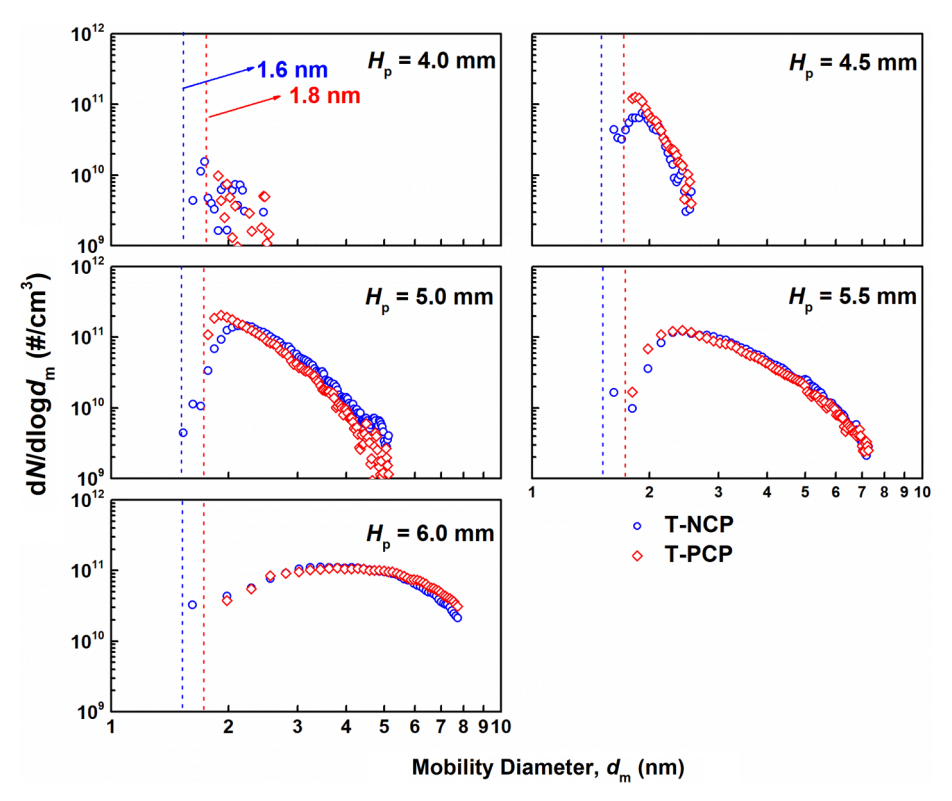


Fig. 2. The total PSDs of Flame A2 inferred from either positively charged particles (T-PCP) or negatively charged particles (T-NCP) measurements at different  $H_p$ . Lines represent cut-off sizes.

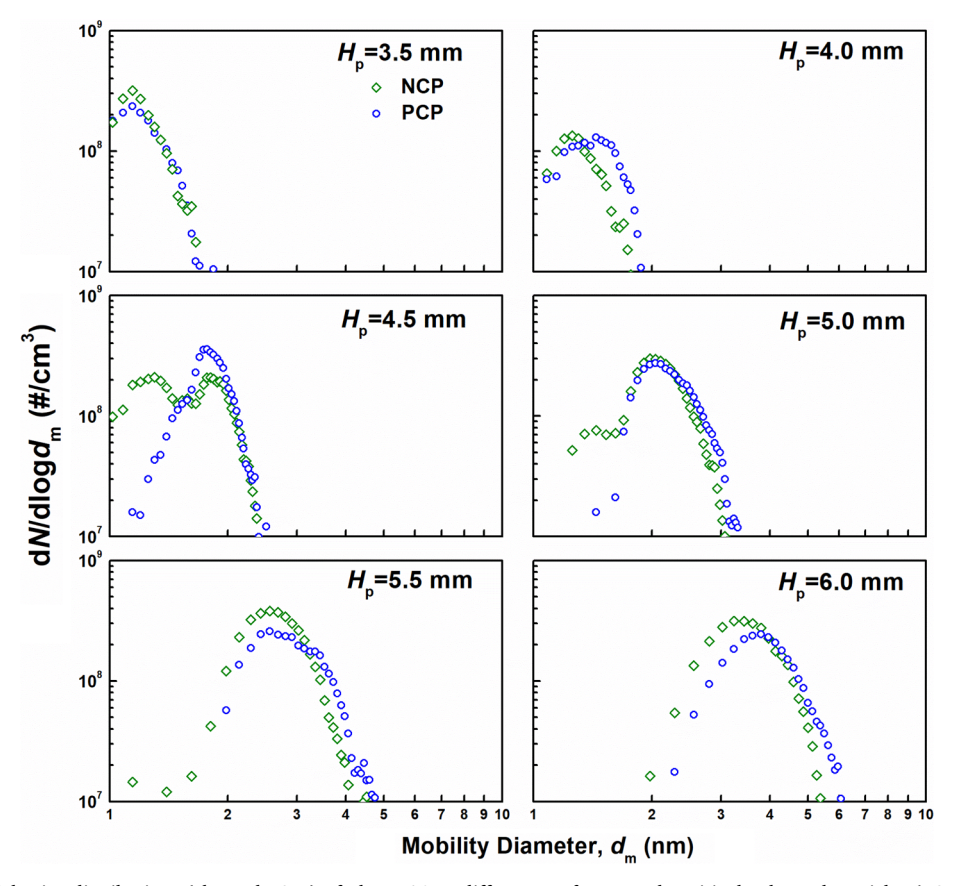


Fig. 3. The charged particle size distributions (charged PSDs) of Flame A2 at different  $H_p$  for natural positively charged particles (PCP) and negatively charged particles (NCP).

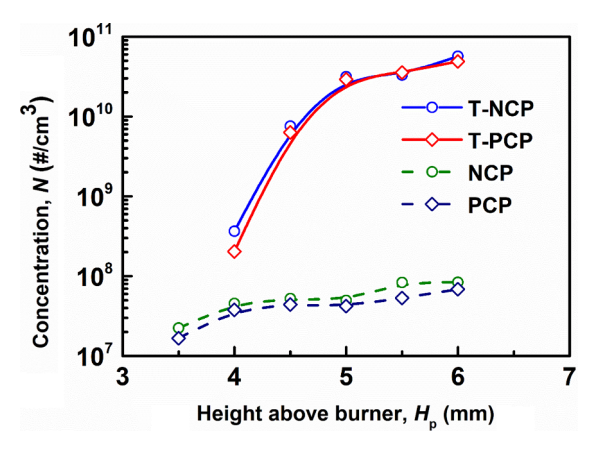


Fig. 4. Number concentrations vs.  $H_p$  for total particles (T-NCP and T-PCP) and charged particles (NCP and PCP).

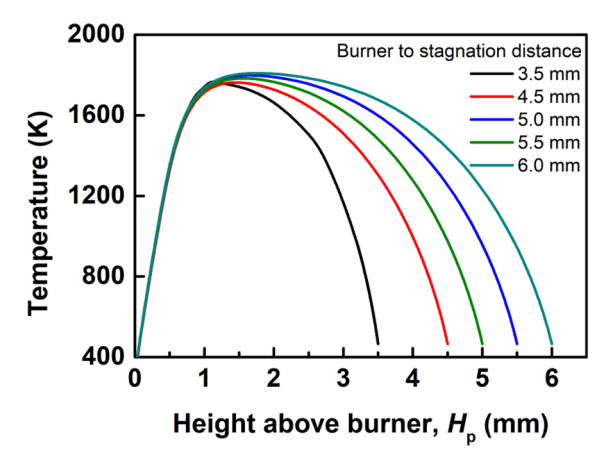


Fig. 5. The computed temperature profiles of Flame A2 at different  $H_p$ .

 $H_{\rm p}$ , the sampled particles were mainly generated near the flame front. This was reasonable as more ions could be generated near the flame front, where the temperature was higher, leading to a higher probability to charge soot particles. At high  $H_{\rm p}$ , the total concentrations still increased with the increase of  $H_{\rm p}$  compared to the almost constant concentration of charged particles, which indicated that the newly nucleated soot at high  $H_{\rm p}$  (post-flame region) were all neural. It is worth mentioning that our sampling method did not obviously affect  $T_{\rm max}$ 

when reducing sampling height, as the sampling tube was embedded in the stagnation plate as a flame boundary. In addition, the median diameters of total and charged PSDs were found to increase with  $H_{\rm p}$  as shown in Fig. S4 in the Supplemental Material, indicating particles grew through coagulation. The highly consistent median diameters of total and charged PSDs showed that the growth processes of neutral and charged soot particles were similar and charged PSDs could be correlated to total PSDs to some extent.

For a better comparison of the total and charged sub-10 nm soot particles, Fig. 6 shows the charge fraction as a function of particle mobility diameter. The ratio of the charged PSDs to the total PSDs (T-NCP) was regarded as charge fraction in this work. At  $H_p = 4.5$  mm, the charge fraction decreased with the increase of mobility diameter, indicating the nucleated soot particles carried charges partly. Besides, the charge fraction was the highest at this height, which was likely due to the higher ion concentration near the flame front. As  $H_p$  was increased, the charged particles near the flame front grew to larger particles thus the peak of charge fraction distribution shifted to larger particles as shown at  $H_p = 5.5$  mm and 6.0 mm. An interesting finding was that only nucleated soot particles near the flame front could carry charges while nucleated soot particles in post-flame region were all neutral. Taking 1.6 nm PCP as an example, the charge fraction was almost 0 at  $H_{\rm p}=5.5$  mm and 6.0 mm as shown in Fig. 7. A very likely reason was that ions generated at lower temperatures in the post-stagnation-flame region were too few to charge nucleated soot or to participate in soot nucleation [5,11]. Hence, nucleated soot particles were all neutral at large  $H_p$  and ions had no effect on persistent nucleation. As for larger PCP (2.5 and 3.0 nm), their charge fractions first increased then decreased with the increase of  $H_p$  because nucleated charged particles were formed at low  $H_p$  and then grew to larger particles.

As discussed above, the decrease in charge fraction along  $H_{\rm p}$  in Fig. 6 was likely due to the higher temperature near the flame front. To verify our inference, we investigated the charge characteristics from flames with different  $T_{\rm max}$ , i.e. Flames A1-A3. The evolution of PSDs of T-NCP, T-PCP, NCP and PCP at different  $H_{\rm p}$  can be found in Figs. S5–S8 in the Supplemental Material. The evolution of PSDs of T-NCP, T-PCP for Flames A1 and A3 is similar to that of Flame A2. However, PSDs of Flame A1 showed a remarkable delay of soot formation due to the lower nucleation and mass growth rates in the low temperature flame, while the lower soot concentration of Flame A3 was due to the thermal decomposition of precursors in the high temperature flame [38,39]. Take the case of  $H_{\rm p}=6$  mm as an example. The PSD of T-NCP in Flame A1 peaks at 2 nm with a concentration of  $10^{11}$  cm $^{-3}$ , while in Flame A3 it peaks at  $\sim$ 4.5 nm with a lower concentration of  $\sim 10^{10}$  cm $^{-3}$ . For a better visualized comparison of the variation of total and charged soot

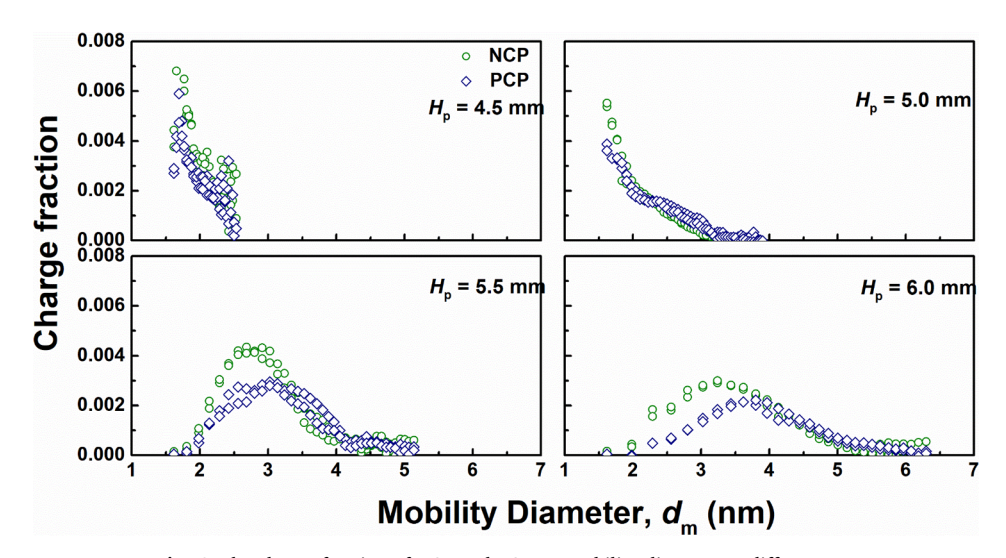


Fig. 6. The charge fraction of NCP and PCP vs. mobility diameter at different  $H_{\mathrm{p}}$ .

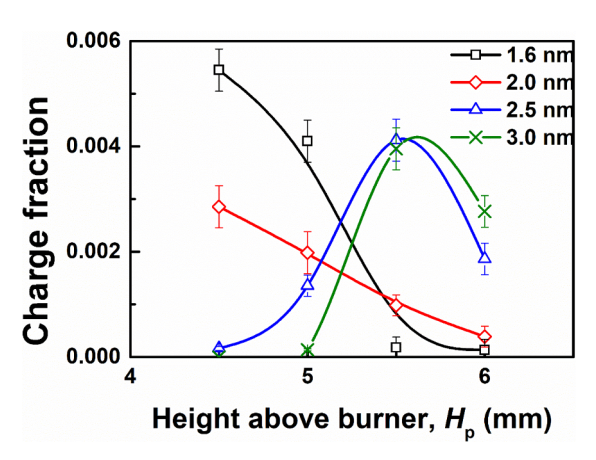


Fig. 7. The charge fraction of PCP vs.  $H_p$  for soot particles with different sizes.

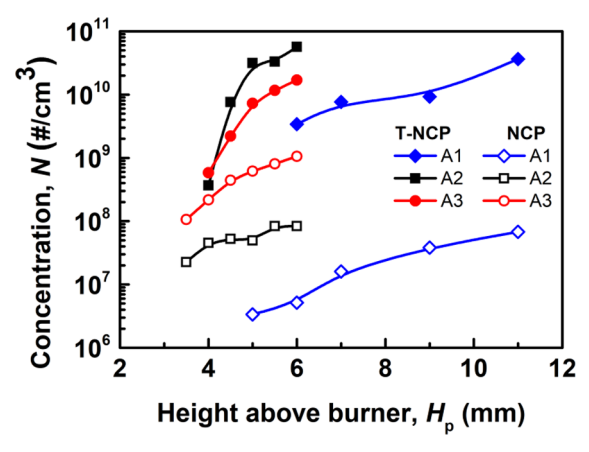


Fig. 8. Number concentrations vs.  $H_{\rm p}$  for total particles (T-NCP) and charged particles (NCP) of Flames A1-A3.

caused by changing flame temperature, Fig. 8 shows the number concentrations of T-NCP and NCP of Flames A1-A3. The total concentrations of soot particles increased first and then decreased with the increase of flame temperature. However, the temperature dependency of the concentrations of NCP was different from that of T-NCP. In the high-temperature Flame A3, the concentrations of charged particle were obviously higher than those of Flames A1 and A2.

The charge fraction shown in Fig. 9 was the ratio of charged PSDs and total PSDs, which showed that when  $T_{\rm max}$  increased from 1665 K to 1933 K, the charge fraction increased by two orders of magnitude (from 10<sup>-3</sup> to 10<sup>-1</sup>), indicating the significant effect of temperature on soot charging. At higher temperatures, more ions were generated and participated in coagulation between soot precursors/nucleated soot and ions, leading to more charged particles. Although the charge fraction increased with temperature, it was still low, thus ion-induced soot nucleation was not the main contributor to soot nucleation in our flames ( $T_{\rm max}$  < 2000 K). However, the ion-induced soot nucleation may become important at higher flame temperatures ( $T_{\rm max} > 2000 \, {\rm K}$ ) if the charge fraction still increases with temperature. Thus, the ionparticle interaction in high temperature flames such as premixed stretch flames [38] may be worthy of study. Besides, since the upper limit of the Half-mini DMA measurements is 10 nm, charge information for larger particles cannot be obtained. In view of the high fraction of larger charged particles reported from a similar premixed ethylene flame [16], incipient nanoparticles are not formed from ion-induced nucleation while the later growth and aggregation could be influenced by ionic effects. Therefore, it is necessary to combine Half-mini DMA and nano-DMA to investigate the charge fraction of 1-80 nm soot particles for understanding how nanoparticles grow into the charged

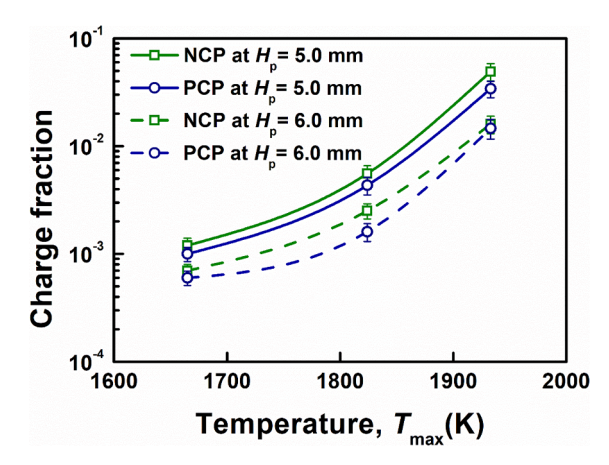


Fig. 9. The charge fraction of NCP and PCP vs.  $T_{\rm max}$  at  $H_{\rm p}=5.0$  and 6.0 mm.

aggregates from uncharged nascent particles.

#### 4. Conclusion

In this study, we investigated the charge characteristics of sub-10 nm soot in premixed ethylene-oxygen–nitrogen flames ( $\Phi=2.0$ ) with varying maximum flame temperatures from 1665 K to 1933 K. The charged and total particle size distributions were measured using a tandem equipment of neutralizer (off or on)-Half-mini DMA-electrometer. The size-dependent charge fractions of sub-10 nm soot at different  $H_{\rm p}$  were analyzed. The charged PSDs showed a lognormal distribution with the peak diameter at 1.2 nm and the smallest positive/negative particles were  $\sim 1$  nm. When measuring the total PSDs, the neutralizer could not charge sub-2 nm soot particles to follow the Fuch's distribution, which was likely due to the low charging efficiency of sub-2 nm soot particles with neutralizer ions. Therefore, the total PSDs data were only reliable for particles with mobility diameters larger than 2 nm.

Our results show at lower  $H_{\rm p}$ , the charge fraction was higher, because both the temperature and ions concentrations were higher near the flame front. By contrast, at higher  $H_{\rm p}$ , the newly nucleated soot was basically neutral. A possible explanation was that at higher temperatures, more ions were generated and participated in coagulation between soot and ions, leading to more charged particles. Since the charge fraction was less than 10% in our flames ( $T_{\rm max} < 2000~{\rm K}$ ), ion-induced soot nucleation was not the main contributor to soot nucleation; however, it may not be neglected at higher flame temperatures ( $T_{\rm max} > 2000~{\rm K}$ ).

#### CRediT authorship contribution statement

Mengda Wang: Conceptualization, Methodology, Data curation, Investigation, Writing - original draft. Girish Sharma: Conceptualization, Methodology, Data curation, Investigation, Writing - review & editing. Huang Zhang: Data curation, Writing - review & editing. Xiaoqing You: Supervision, Resources, Writing - review & editing. Pratim Biswas: Supervision, Resources, Writing - review & editing.

#### **Declaration of Competing Interest**

The authors declare that they have no known competing financial interests or personal relationships that could have appeared to influence the work reported in this paper.

#### Acknowledgement

This work was supported by the National Natural Science Foundation of China (51761125012) and a grant from the National Science Foundation, SusChEM: Ultrafine Particle Formation in Advanced Low Carbon Combustion Processes; CBET 1705864. Girish Sharma would like to thank McDonnell International Academy at Washington University in St Louis for their support.

#### Appendix A. Supplementary data

Supplementary data to this article can be found online at https:// doi.org/10.1016/i.fuel.2020.118511.

#### References

- [1] Frenklach M. Reaction mechanism of soot formation in flames. Phys Chem Chem Phys 2002;4(11):2028-37. https://doi.org/10.1039/b110045a
- Fialkov A. Investigations on ions in flames. Prog Energy Combust Sci 1997;23(5-6):399-528. https://doi.org/10.1016/s0360-1285(97)00016-6.
- Goodings JM, Bohme DK, Ng C-W. Detailed ion chemistry in methane-oxygen flames. I. Positive ions. Combust Flame 1979;36:27-43. https://doi.org/10.1016/ 0010-2180(79)90044-0.
- Goodings JM, Bohme DK, Ng C-W. Detailed ion chemistry in methane-oxygen flames. II. Negative ions. Combust Flame 1979;36:45-62. https://doi.org/10.1016/
- [5] Mätzing H, Baumann W, Bockhorn H, Paur H-R, Seifert H. Detection of electrically charged soot particles in laminar premixed flames. Combust Flame 2012;159(3):1082-9. https://doi.org/10.1016/j.combustflame.2011.09.014.
- Carbone F, Canagaratna MR, Lambe AT, Jayne JT, Worsnop DR, Gomez A. Exploratory analysis of a sooting premixed flame via on-line high resolution (APi-TOF) mass spectrometry. Proc Combust Inst 2019;37(1):919-26. https://doi. org/10.1016/j.proci.2018.08.020.
- Wang Y, Sharma G, Koh C, Kumar V, Chakrabarty R, Biswas P. Influence of flamegenerated ions on the simultaneous charging and coagulation of nanoparticles during combustion. Aerosol Sci Tech 2017;51(7):833-44. https://doi.org/10.1080/ 02786826.2017.1304635.
- Zhang Y, Li S, Yan W, Yao Q, Tse SD. Role of dipole-dipole interaction on enhancing Brownian coagulation of charge-neutral nanoparticles in the free molecular regime. J Chem Phys 2011:134(8):084501https://doi.org/10.1063/1.3555633.
- Sharma G, Wang Y, Chakrabarty R, Biswas P. Modeling simultaneous coagulation and charging of nanoparticles at high temperatures using the method of moments. J Aerosol Sci 2019;132:70-82. https://doi.org/10.1016/j.jaerosci.2019.03.011.
- Starik AM, Savel'ev AM, Titova NS. Formation of charged nanoparticles in hydrocarbon flames: principal mechanisms. Plasma Sources Science and Technology 2008;17(4). doi: 10.1088/0963-0252/17/4/045012.
- [11] Calcote HF, Olson DB, Keil DG. Are ions important in soot formation? Energy Fuel 1988;2(4):494-504. doi: 10.1021/ef00010a016.
- Calcote HF. Mechanisms of soot nucleation in flames—a critical review. Combust Flame 1981;42:215-42. https://doi.org/10.1016/0010-2180(81)90159-0.
- [13] Martin JW, Bowal K, Menon A, Slavchov RI, Akroyd J, Mosbach S, et al. Polar curved polycyclic aromatic hydrocarbons in soot formation. Proc Combust Inst 2019;37(1):1117-23. https://doi.org/10.1016/j.proci.2018.05.046.
- [14] Bowal K, Martin JW, Misquitta AJ, Kraft M. Ion-induced soot nucleation using a new potential for curved aromatics. Combust Sci Technol 2019;191(5-6):747-65. https://doi.org/10.1080/00102202.2019.1565496.
- [15] Haynes BS, Wagner HG. Soot formation. Prog Energy Combust 1981;7(4):229-73. https://doi.org/10.1016/0360-1285(81)90001-0.
- [16] Maricq MM. Size and charge of soot particles in rich premixed ethylene flames. Combust Flame 2004;137(3):340-50. https://doi.org/10.1016/j.combustflame. 2004.01.013
- [17] Fernández de la Mora J, Kozlowski J. Hand-held differential mobility analyzers of high resolution for 1-30 nm particles: Design and fabrication considerations. J Aerosol Sci 2013;57:45-53. https://doi.org/10.1016/j.jaerosci.2012.10.009.
- [18] Zhang H, Sharma G, Wang Y, Li S, Biswas P. Numerical modeling of the

- performance of high flow DMAs to classify sub-2 nm particles. Aerosol Sci Technol 2018;53(1):106-18. https://doi.org/10.1080/02786826.2018.1549358
- [19] Sgro LA, D'Anna A, Minutolo P. Charge distribution of incipient flame-generated particles. Aerosol Sci Technol 2010;44(8):651-62. https://doi.org/10.1080/ 02786826.2010.483701.
- [20] Sgro LA, D'Anna A, Minutolo P. Charge fraction distribution of nucleation mode particles: New insight on the particle formation mechanism. Combust Flame 2011;158(7):1418–25. https://doi.org/10.1016/j.combustflame.2010.11.010.
- Fernandez de la Mora J. High-resolution mobility analysis of charge-reduced electrosprayed protein ions. Anal Chem 2015;87(7):3729-35. https://doi.org/10.1021/
- [22] Fernandez de la Mora J. Expanded flow rate range of high-resolution nanoDMAs via improved sample flow injection at the aerosol inlet slit. J Aerosol Sci 2017;113:265-75. https://doi.org/10.1016/j.jaerosci.2017.07.020.
- Wang Y, Kangasluoma J, Attoui M, Fang J, Junninen H, Kulmala M, et al. The high charge fraction of flame-generated particles in the size range below 3 nm measured by enhanced particle detectors. Combust Flame 2017;176:72-80. https://doi.org/ 10.1016/j.combustflame.2016.10.003.
- [24] Wang Y, Kangasluoma J, Attoui M, Fang J, Junninen H, Kulmala M, et al. Observation of incipient particle formation during flame synthesis by tandem differential mobility analysis-mass spectrometry (DMA-MS). Proc Combust Inst 2017;36(1):745-52. https://doi.org/10.1016/j.proci.2016.07.005.
- Carbone F, Attoui M, Gomez A. Challenges of measuring nascent soot in flames as evidenced by high-resolution differential mobility analysis. Aerosol Sci Technol 2016;50(7):740-57. https://doi.org/10.1080/02786826.2016.1179715
- Wang M, Tang Q, Mei J, You X. On the effective density of soot particles in premixed ethylene flames. Combust Flame 2018;198:428-35. https://doi.org/10. 1016/j.combustflame.2018.10.004.
- Camacho J, Liu C, Gu C, Lin H, Huang Z, Tang Q, et al. Mobility size and mass of nascent soot particles in a benchmark premixed ethylene flame. Combust Flame
- 2015;162(10):3810-22. https://doi.org/10.1016/j.combustflame.2015.07.018. Tang Q, Mei J, You X. Effects of CO 2 addition on the evolution of particle size distribution functions in premixed ethylene flame. Combust Flame 2016;165:424–32. https://doi.org/10.1016/j.combustflame.2015.12.026.
- Abid AD, Camacho J, Sheen DA, Wang H. Quantitative measurement of soot particle size distribution in premixed flames – the burner-stabilized stagnation flame approach. Combust Flame 2009;156(10):1862-70. https://doi.org/10.1016/j. combustflame 2009 05 010
- Fuchs NA. On the stationary charge distribution on aerosol particles in a bipolar ionic atmosphere. Geofis Pura Appl 1963;56(1):185–93. https://doi.org/10.1007/ bf01993343.
- Reaction Workbench 15131, Reaction Design: San Diego. http://www.reactionde-
- sign.com/support /help/help\_usage\_and\_support/how-to-cite-products/.
  Wang H, You X, Joshi AV, Davis SG, Laskin A, Egolfopoulos F, Law CK, USC Mech Version II. High-Temperature Combustion Reaction Model of H2/CO/C1-C4 Compounds. http://ignis.usc.edu/USC\_Mech\_II.htm, May 2007.
- Wiedensohler A. An approximation of the bipolar charge distribution for particles in the submicron size range. J Aerosol Sci 1988;19(3):387-9. doi: 10.1016/0021-8502(88)90278-9.
- Wiedensohler A, Fissan HJ. Bipolar charge distributions of aerosol particles in highpurity argon and nitrogen. Aerosol Sci Technol 1991;14(3):358-64.
- Reischl GP, Mäkelä JM, Karch R, Necid J. Bipolar charging of ultrafine particles in the size range below 10 nm. J Aerosol Sci 1996;27(6):931-49. https://doi.org/10. 1016/0021-8502(96)00026-2.
- Ziemann PJ, Kittelson DB, McMurry PH. Effects of particle shape and chemical composition on the electron impact charging properties of submicron inorganic particles. J Aerosol Sci 1996;27(4):587-606. https://doi.org/10.1016/0021-8502(96)00010-9.
- [37] Romay FJ, Pui DYH. Free electron charging of ultrafine aerosol particles. J Aerosol Sci 1992;23(7):679-92. https://doi.org/10.1016/0021-8502(92)90036-u
- Camacho J, Singh AV, Wang W, Shan R, Yapp EKY, Chen D, et al. Soot particle size distributions in premixed stretch-stabilized flat ethylene-oxygen-argon flames Proc Combust Inst 2017;36(1):1001-9. https://doi.org/10.1016/j.proci.2016.06.
- Abid AD, Heinz N, Tolmachoff ED, Phares DJ, Campbell CS, Wang H. On evolution of particle size distribution functions of incipient soot in premixed ethylene-oxygen-argon flames. Combust Flame 2008;154(4):775-88. doi: 10.1016/j.combustflame.2008.06.009.